

Soft Matter

Accepted Manuscript



This is an *Accepted Manuscript*, which has been through the Royal Society of Chemistry peer review process and has been accepted for publication.

Accepted Manuscripts are published online shortly after acceptance, before technical editing, formatting and proof reading. Using this free service, authors can make their results available to the community, in citable form, before we publish the edited article. We will replace this *Accepted Manuscript* with the edited and formatted *Advance Article* as soon as it is available.

You can find more information about *Accepted Manuscripts* in the [Information for Authors](#).

Please note that technical editing may introduce minor changes to the text and/or graphics, which may alter content. The journal's standard [Terms & Conditions](#) and the [Ethical guidelines](#) still apply. In no event shall the Royal Society of Chemistry be held responsible for any errors or omissions in this *Accepted Manuscript* or any consequences arising from the use of any information it contains.



Journal Name

ARTICLE

Heterogeneity of Single-Colloid Self-Potentials at an Oil-Water Interface

Mina Lee^a and Bum Jun Park^{a*}Received 00th January 20xx,
Accepted 00th January 20xx

DOI: 10.1039/x0xx00000x

www.rsc.org/

Heterogeneity in the interactions between colloidal particles at an oil-water interface is explored on a single particle level. Such a characteristic arises due to heterogeneity in self-potentials that individual particles possess. Energy minimization is numerically performed to determine the self-potentials of single colloids when the interface-trapped particles form uniquely arranged structures. We demonstrate that the obtained self-potentials correspond to the dipole strength of individual particles at the interface that can be attributed to the generation of abnormally strong and long-range repulsive interactions that should also be heterogeneous. The characterization of self-potentials on a single-particle level can potentially provide insight into the origin of heterogeneity of colloidal suspension systems at multiphase fluid interfaces. Furthermore, the findings obtained here may facilitate an understanding of the hierarchical relationships associated with scale-dependent colloidal particle behaviors that arise due to interaction heterogeneity.

Introduction

Heterogeneity is ubiquitous in myriad colloid systems and plays an important role in various phenomena, including electrolyte or gas adsorption, transport through porous media, particle packing, suspension structure, and rheology.¹⁻⁷ Such heterogeneities may originate from the surface structure, surface-attached impurities, porosity, and the non-uniform distribution of functional groups on the surface of colloids.⁸⁻¹⁰ The heterogeneity of particle interactions in a colloidal suspension is a significant and complex factor, as the assumption of homogeneous interparticle interactions can lead to inaccurate predictions of the structural and rheological properties of a suspension composed of identical particles.^{11,12} Despite the critical importance of heterogeneity in terms of material properties, only a few efforts have been devoted to understanding the intimate relationships associated with scale-dependent hierarchical particle behaviors that arise from interaction heterogeneity.^{11,13} Such a scenario has served as motivation to investigate the heterogeneity of single-particle interaction potentials, which we call *self-potentials*.

Optical laser tweezers are typically employed to measure the piconewton forces between two interacting colloidal particles.^{14,15} The magnitude of the measured two-particle or pair interactions is known to be heterogeneous when the particles are trapped at a fluid-fluid interface. However, strictly

speaking it is more accurate to state that the magnitude of the interaction potential that each interacting particle possesses is heterogeneous. Measurement of such single particle potentials (i.e., self-potentials) is not a trivial matter. To the best of our knowledge, there has been no attempts to quantitatively study and characterize heterogeneous interaction potentials on a single-particle level.

In this work, we develop the method to characterize the self-potential for a colloidal system with particles trapped at a fluid-fluid interface. The role of heterogeneity of the self-potentials in the assembly of particles at the fluid-fluid interface is also investigated. Finally, the physical meaning of the self-potential is elucidated. Colloidal particles typically adsorb strongly to a fluid-fluid interface and the magnitude of colloid interactions at the interface is approximately thousands of times higher than that between identical particles dispersed in a single fluid medium.¹⁶⁻²¹ Interface-trapped colloidal systems can be utilized in numerous applications related to food, pharmaceuticals, cosmetics, oil recovery, and biofuel conversion processes.²¹⁻²⁷ Furthermore, it has recently been noted that control over the assembly of particles with versatile functionalities at fluid interfaces can be used to establish micro- and nano-scale building blocks, thereby providing unprecedented possibilities for the construction of hierarchical suprastructures and functional materials with desired properties.²⁸⁻³³ It is thus important to recognize that the characteristics of building block components (e.g., self-potentials and heterogeneity) on a single-particle level intrinsically affect the macroscopic behavior and properties of designed materials.

^a Department of Chemical Engineering, Kyung Hee University, Yongin, 446-701, South Korea

† Corresponding author: Bum Jun Park: (Tel) +82-31-201-2429, (email) bjpark@khu.ac.kr

Experimental

Polystyrene (PS) particles with a diameter of $2R \approx 200 \mu\text{m}$ were prepared via a co-flow microfluidic method in which 30 wt% polystyrene (M.W = 190K, Sigma-Aldrich) in methylene chloride (Sigma-Aldrich) was supplied to an inlet capillary channel and 2 wt% polyvinyl alcohol (PVA, Sigma-Aldrich) in water was provided to a co-axial capillary channel.³⁴ The polymer solution flowing out of the orifice forms microdroplets in the PVA aqueous solution that were collected in pure water. The obtained polystyrene droplets were dried at ambient temperature for several days and were washed using pure water several times to remove the excess PVA. The surface charge was determined to be approximately -20mV (Beckman Coulter Delsa Nano-C) due to surface-attached PVA groups.³⁴

An oil lens was formed by gently placing a small amount of *n*-decane on the surface of water (resistivity > 18.2 M Ω -cm).³⁴ A particle was gently placed outside the oil lens at the air-water interface using a micropipette. The particle initially at the air-water interface were spontaneously transported through the air-water-oil triple phase boundary and moved toward the center of the oil lens along the curved oil-water interface. We previously demonstrated the detailed mechanism of the spontaneous transport behaviors of a spherical particle through an air-water-oil triple-fluid phase boundary.³⁴ There are two distinct transport regimes: a particle accelerates upon its spontaneous adsorption to the triple phase boundary (capillarity regime), and subsequently, decelerates after detaching from the triple phase boundary (relaxation regime). The driving force for the acceleration in the capillarity regime can be attributed to the gradient in the attachment energy of the particle to multiple fluid-fluid interfaces (i.e., air-water, air-oil, and oil-water interfaces) present around the triple phase boundary. The particle slows down in the relaxation regime due to the drag force of the surrounding fluids and consequently collects at the bottom of the oil lens. Note that local interface deformation around the particle due to gravity is negligible because the Bond number, which is the ratio of gravitational force to the interfacial tension force, is sufficiently small ($Bo \approx 10^{-3}$), and thus, the interface deformation-induced capillary force between the particles seldom occurs. After introducing the particles, the sample cell was covered to minimize evaporation and convection. A CCD camera (Hitachi KP-M1AN) was employed to capture microscopic images of the particles at the oil-water interface.

Results and Discussion

Particles trapped at the curved interface are balanced by electrostatic repulsion (U_{rep}) and the potential energy ($U_{pot} = U_{gravity} + U_{buoyancy}$) due to gravity and buoyancy (Fig. 1a). The typical electrostatic repulsion between two particles at a planar fluid-fluid interface can be represented by $U_{rep}/k_B T = a/r^3$, where a is the magnitude of the pair interaction, k_B is Boltzmann's constant, T is temperature, and r is the center-

to-center separation between the particles.^{16, 19, 35, 36} The curvature radius of the oil-water interface in the oil lens system is sufficiently large compared to the particle size and thus, the scaling behavior of the repulsive interaction reasonably depicts particle interactions at such curved interfaces. Particles tend to settle at the bottom of the curved oil-water interface due to gravity. The corresponding potential energy of two particles when incorporating gravity and buoyancy is given by $U_{pot}/k_B T = g(\rho_p V_p - \rho_w V_{pw} - \rho_o V_{po})(h_1(\lambda) + h_2(\lambda))$, where λ is the radial distance from the center of the oil lens, V_p is the volume of a particle, ρ is the density, g is the acceleration due to gravity, and h_1 and h_2 are the vertical distances of the two particles from the bottom of the oil lens (Fig. 1a). The subscripts p , w , and o denote the particle, water, and oil, respectively. Using geometric relations, the particle volumes immersed in each fluid phase are $V_{pw} = \frac{\pi R^3}{3}(2 + 3\cos\theta_c - \cos^3\theta_c)$ in water and $V_{po} = \frac{\pi R^3}{3}(2 - 3\cos\theta_c + \cos^3\theta_c)$ in oil. The three-phase contact angle ($\theta_c = 105^\circ$) of a particle at the oil-water interface was measured via the gel-trapping method.³⁷ The interface height, $h(\lambda)$, where a particle is located was acquired by interpolation of $z(\lambda)$ at a given value of λ (Fig. 1b). The shape of the oil lens (air-water, air-oil, and oil-water interfaces) in Fig. 1b was obtained according to a previously reported method in which the spreading coefficient of *n*-decane is $S_{oil} = -3.72$.³⁸ When the electrostatic repulsion and potential energy of two particles are in equilibrium, the particles rest at an equilibrium height ($h_{eq}(\lambda) = h_1 = h_2$) with an equilibrium separation ($r_{eq} = 2\lambda_{eq}$), as displayed in Fig. 1a.

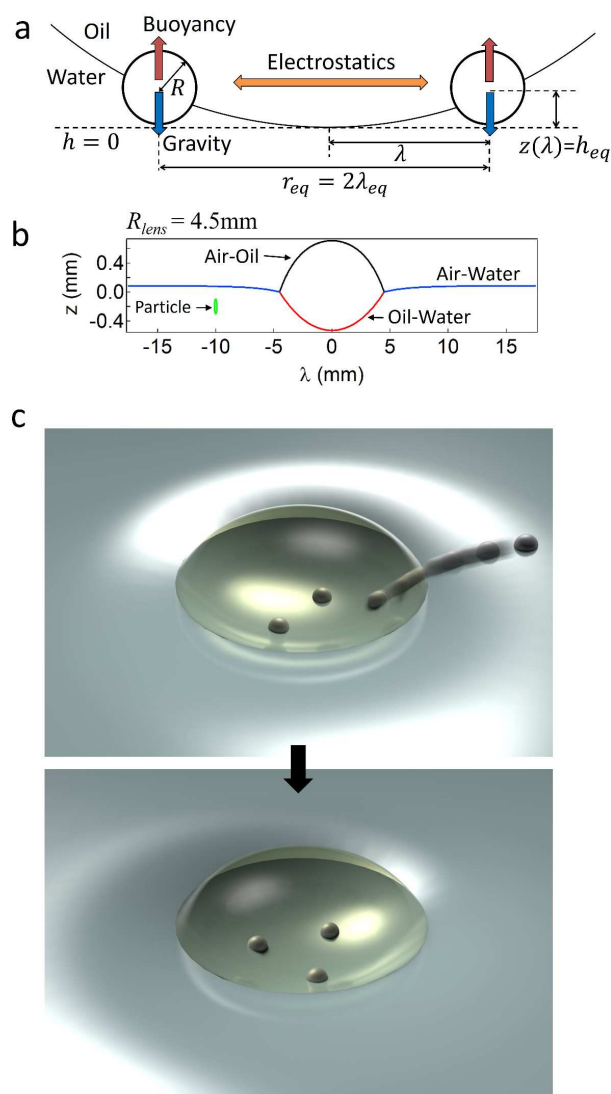


Fig. 1 Schematic of the measurement strategy to determine the self-potentials of individual particles at a curved oil-water interface. (a) Two interacting particles with an equilibrium separation (r_{eq}) at the interface. (b) Shape of the oil lens on the water surface. (c) Schematics of particle transfer and adsorption toward the oil lens (i.e., at oil-water interface).

When considering three particles at the curved oil-water interface, three independent conditions are required to determine their self-potentials ($\Omega_1, \Omega_2, \Omega_3$): (1) the pair interaction ($a_{12} = \Omega_1\Omega_2$) between particles 1 and 2 when only two particles reside at the interface (Fig. 3a), (2) the positions of three particles (r_1, r_2, r_3), which tend to form a triangular structure, upon adding a third particle to the interface (Fig. 2 and Fig. 3b), and (3) the condition that the triangular structure corresponds to a state of minimum energy, $U_{min} = \min(U_{rep} + U_{pot})$. The self-potentials of additional particles are subsequently obtained by adding particles one after another (Fig. 3c-e).

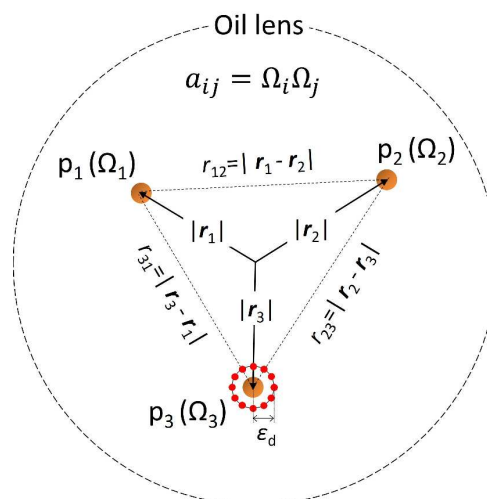


Fig. 2 Geometry of three particles (yellow circles) forming a triangular structure; the dashed circle indicates the boundary of the oil lens.

To determine the pair interaction magnitude (a_{12}) between two particles (p_1 and p_2), the net interaction energy ($U_{net} = U_{rep} + U_{pot}$) is calculated as a function of the particle separation when the values of a and V_{oil} are changed.¹³ Since the electrostatic repulsion (U_{rep}) decays as r^{-3} and the potential energy (U_{pot}) monotonically increases with r , a minimum (U_{min}) in the net energy curve exists at an equilibrium separation of r_{eq}/R for a corresponding value of a at a given V_{oil} . The value of a_{12} can then be determined by comparing the calculated r_{eq}/R to the experimentally obtained equilibrium separation (Fig. 3a).

Next, we calculate the net interaction energy ($U_{net}^0 = U_{rep}^0 + U_{pot}^0$) after introducing a third particle (p_3) to the interface. The superscript "0" indicates an equilibrium state in which the three particles are organized into a triangular structure with position vectors, $\mathbf{r}_1, \mathbf{r}_2$, and \mathbf{r}_3 from the center of the oil lens (Fig. 2). These vectors can be obtained from the image shown in Fig. 3b. Bold letters indicate vectors or matrices in this work. The term U_{pot}^0 denotes the sum of the potential energy of the three particles at equilibrium, while U_{rep}^0 represents the total electrostatic interactions among the three particles. Based on pairwise additivity, U_{rep}^0 can be calculated from $\frac{U_{rep}^0}{k_B T} = \frac{A_{12}}{r_{12}^3} + \frac{A_{23}}{r_{23}^3} + \frac{A_{31}}{r_{31}^3}$, where r_{ij} is the interparticle separation between particles i and j , $r_{ij} = |\mathbf{r}_i - \mathbf{r}_j|$, and \mathbf{A}_{ij} is a $(n \times n)$ matrix composed of pair interaction magnitudes. Here, $\mathbf{A}_{12} = a_{12} \times \mathbf{J}_n$, $\mathbf{A}_{23} = \Omega_2 \times \Omega_3$, and $\mathbf{A}_{31} = \Omega_3 \times \Omega_1$, where \mathbf{J}_n is a matrix of ones with n -by- n dimensions; the period before the multiplication sign indicates element-wise multiplication. A large number of n is used to improve the accuracy of the calculations (i.e., $n = 1500$). The $(n \times n)$ matrix of self-potentials (Ω_1) for p_1 consists of n row vectors $[\Omega_{min}, \dots, \Omega_{max}]$ with $(1 \times n)$ dimensions. Furthermore, $\Omega_{min} = 2 \times 10^3$ and $\Omega_{max} = 3 \times 10^4$ ($\text{pN} \cdot \mu\text{m}/R^3$)^{1/2} are sufficiently

small and large values of the self-potential, respectively, so that $a_{min} \gg \Omega_{min}^2$ and $a_{max} \ll \Omega_{max}^2$, where a_{min} and a_{max} are the minimum and maximum values of the measured pair interaction magnitude. The self-potential of p_2 depends on the pair interaction magnitude (a_{12}) and thus, $\Omega_2 = a_{12}/\Omega_1$. For p_3 , the corresponding matrix of the self-potential is given by $\Omega_3 = \Omega_1^T$, where the superscript T indicates the transposition of a matrix. Consequently, elements of the ($n \times n$) matrix U_{net}^0 represent all possible combinations of net interaction potentials resulting from $\Omega = [\Omega_{min}, \dots, \Omega_{max}]$ when the three particles are in an equilibrium configuration (r_1, r_2, r_3). The position of p_3 is subsequently displaced by ϵ_d , as indicated by the red dots in Fig. 2, and the net potentials U_{net}^k ($k = 1, 2, 3, \dots, 12$) are repeatedly calculated according to the same procedure. Subtraction of the net interaction energy of the perturbed configurations from that of the equilibrium state, $\Delta U_{net} = U_{net}^0 - U_{net}^k$, yields $k \times (n \times n)$ matrices. Finally, the row and column indices (l, m) that satisfy the condition of $\Delta U_{net} < 0$ through all k matrices correspond to the values of the self-potential, i.e., $\Omega_1 = \Omega_1(l, m)$, $\Omega_2 = \Omega_2(l, m)$, and $\Omega_3 = \Omega_3(l, m)$. Notably, this perturbation method eliminates all possible self-potentials that tend to displace the third particle to surroundings in which the net interaction energy decreases ($U_{net}^0 > U_{net}^k$).

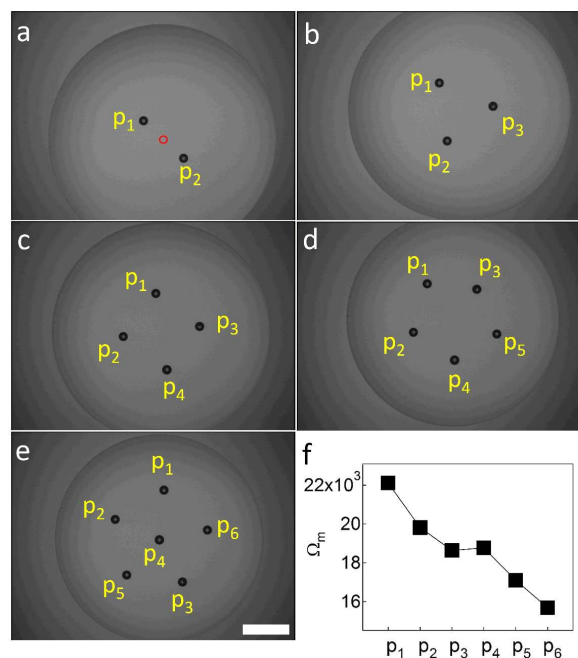


Fig. 3 Determination of the self-potentials. (a-e) Microscopic images of the particles at the curved oil-water interface. Particles were added to the oil lens one after another. The red circle in panel-a indicates the center of the oil lens; the scale bar is 1 mm. (f) Self-potentials (Ω_m) acquired for six particles.

Once the self-potentials ($\Omega_1, \Omega_2, \Omega_3$) of the three particles are determined, obtaining the self-potential (Ω_4) of a fourth particle (p_4) added to the interface is rather straightforward. The four particles form a quadrangular structure with the position vectors r_1, r_2, r_3 , and r_4 at equilibrium (Fig. 3c). In this case, the electrostatic interactions among the four particles are given by $\frac{U_{rep}^0}{k_B T} = \frac{A_{12}}{r_{12}^3} + \frac{A_{23}}{r_{23}^3} + \frac{A_{31}}{r_{31}^3} + \frac{A_{14}}{r_{14}^3} + \frac{A_{24}}{r_{24}^3} + \frac{A_{34}}{r_{34}^3}$, while the pair interaction magnitudes are $A_{12} = \Omega_1 \Omega_2 \times J_n$, $A_{23} = \Omega_2 \Omega_3 \times J_n$, $A_{31} = \Omega_3 \Omega_1 \times J_n$, $A_{14} = \Omega_1 \times \Omega_4$, $A_{24} = \Omega_2 \times \Omega_4$, and $A_{34} = \Omega_3 \times \Omega_4$; the ($n \times n$) matrix of Ω_4 for p_4 is composed of n row vectors $[\Omega_{min}, \dots, \Omega_{max}]$ with $(1 \times n)$ dimensions. The same perturbation method is employed to find the row and column indices (l, m) in which the corresponding self-potential ($\Omega_4 = \Omega_4(l, m)$) satisfies the condition of $\Delta U_{net} < 0$ over all trials of displacements of p_4 . A similar procedure is used to determine the self-potentials after adding more particles one after another (Fig. 3d and 3e).

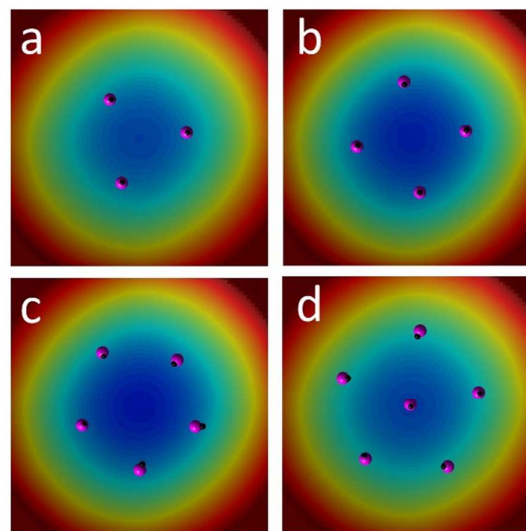


Fig. 4 Comparison of experimental (black dots) findings and MC simulation (pink dots) results based on the obtained values of Ω_m .

The obtained self-potentials show heterogeneity that depends on the individual particles. This heterogeneity directly affects the assembled structures formed by the particles. As shown in Fig. 3f, the values of the self-potentials for six particles varies from 15.67×10^3 to 22.11×10^3 ($\text{pN} \cdot \mu\text{m}/\text{R}^3$)^{1/2}. To validate the accuracy of the calculations, we conducted MC simulations in which the self-potentials in Fig. 3f were introduced ($U_{rep,ij}/k_B T = a_{ij}/r_{ij}^3 = \Omega_1 \Omega_2 / r_{ij}^3$). The particle positions extracted from Fig. 3b-e were used as the initial conditions in the simulations. Assuming pairwise additivity, the net interaction energy of an individual particle i corresponds to the sum of all pair interactions with the other particles and the potential

energy, $U_{net,i} = U_{pot,i} + \sum_j^N U_{rep,ij}$ ($i \neq j$). Note that the pairwise additivity of the interaction potentials was previously justified when the interparticle interactions are sufficiently strong and long-ranged (i.e., electrostatic repulsions between particles at fluid-fluid interfaces).³⁹ The total energy of N particles' configurations can then be expressed as $U_{tot} = \sum_j^N U_{net,i}$ ($i < j$). As shown in the experimental configurations (black dots) of Fig. 4a-d, three to six particles form a triangle, quadrangle, pentagon, and pentagon with one inner particle, respectively. The experimental configurations were overlaid on those derived from simulations (pink dots) for the cases of $N = 3 - 6$. Excellent agreement was observed between the two sets of results, thereby demonstrating that the obtained self-potential values are reasonable.

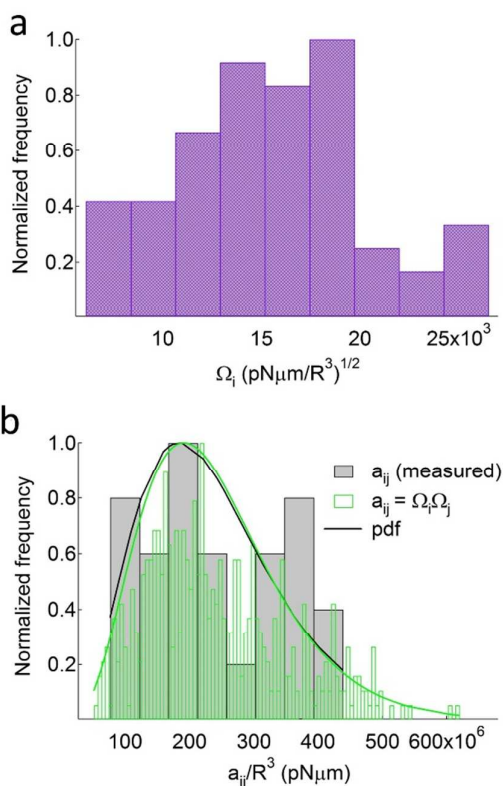


Fig. 5 Histograms of (a) the obtained self-potentials for 60 particles and (b) the magnitude of the pair interactions. Grey bars indicate the measured interaction magnitude for 25 particle pairs, while green bars represent the pair interaction magnitude obtained with random combinations (500 trials) of the self-potentials in panel-a. The solid curves denote the normalized probability density function (pdf).

The validity of the self-potentials was also confirmed by a comparison with measured pair interaction magnitudes. The obtained self-potentials for 60 particles in Fig. 5a were randomly combined to yield the pair interaction magnitude,

$a_{ij} = \Omega_i \Omega_j$; the resulting histogram is shown by green bars in Fig. 3b. From the random combinations, it was determined that a_{ij} follows a gamma distribution $f(a; k, \theta) = a^{k-1} \frac{e^{-a/\theta}}{\theta^k \Gamma(k)}$ with shape and scale parameters of $k = 4.36$ and $\theta = 5.48 \times 10^7$ pN $\cdot\mu\text{m}/\text{R}^3$, respectively. The measured pair interaction magnitude, as indicated by the grey bars in Fig. 5b, also followed a gamma distribution. The shape and scale parameters ($k = 4.83$ and $\theta = 5.00 \times 10^7$ pN $\cdot\mu\text{m}/\text{R}^3$, respectively) were similar to the values obtained using random combinations. The good agreement between the two results confirms that the method of determining the self-potential is quite effective.

Finally, the physical meaning of the self-potential was investigated. It is known that electrostatic repulsions between colloidal particles at a fluid-fluid interface are unusually strong when compared to electrostatic double layer interactions between identical particles dispersed in a single fluid medium (e.g., water). Such strong electrostatic repulsions at the interface can be attributed to dipolar repulsion in which charge dissociation and the asymmetric counterion distribution around each particle in the aqueous phase create a dipole perpendicular to the interface.^{19, 20, 35} Electrostatic repulsions at the interface may also arise due to residual surface charges in the nonpolar phase (e.g., oil or air) that can be dissociated and stabilized by a small amount of water captured in cavities at the particle surface.^{16, 17} In this case, charges in the oil phase induce image charges in the aqueous phase and thus, dipole-like interactions are also responsible for the strong repulsion. Despite the absence of a consensus regarding the mechanism of electrostatic repulsion, experimental and theoretical studies consistently show scaling behavior of $U_{rep} \sim r^{-3}$ that likely originates from dipolar characteristics. The dipole-induced interactions between particles i and j can be expressed as $\frac{U_{dipole,ij}}{k_B T} = K \frac{M_i M_j}{r_{ij}^3}$, where M is the dipole strength and K is a factor of proportionality. A comparison of this dipole-based expression to $\frac{U_{rep,ij}}{k_B T} = \frac{\Omega_i \Omega_j}{r_{ij}^3}$, leads to a simple but crucial observation: the self-potential is proportionally related to the dipole strength of particles at the interface ($\Omega \sim M$) and is therefore, heterogeneous.

Conclusions

The interaction heterogeneity between particles at an oil-water interface was investigated. Such a characteristic arises due to heterogeneity in the self-potentials that the individual particles possess. The self-potentials could be determined by establishing an energy balance when the particles are trapped at a curved oil-water interface; the electrostatic repulsion between the particles is balanced with the potential energy due to gravity and buoyancy. We confirmed that the devised method of determining self-potentials is feasible and accurate by comparing experimental assembly structures to those from

MC simulations when the obtained self-potentials are introduced. Moreover, random combinations of the self-potentials lead to a gamma distribution that is remarkably consistent with the distribution of the measured pair interaction magnitudes. Notably, it was found that the measured self-potentials correspond to the dipole strength of the particles at the interface, which can account for the abnormally strong and long-ranged repulsive interactions between the particles. It remains unclear whether the contribution of charge effects in each fluid phase has a significant effect on the observed strong electrostatic repulsions, and further quantitative studies are required to reveal the exact mechanism of dipole formation. In addition, the presence of many particles at the curved interface likely alters assembly patterns and the diversity of assembly structures, and thus, such complex behaviors of the many particle systems warrant future investigation. Regardless, characterization of the self-potentials of individual particles may provide insight into the origin of heterogeneity of various colloidal suspension systems at the immiscible fluid-fluid interfaces. Such an understanding may also allow for the structure and properties of materials constructed by colloidal systems to be designed and engineered via directed assembly techniques.

Acknowledgements

M.L. and B.J.P. acknowledge funding from the Basic Science Research Program of the National Research Foundation (NRF) of Korea funded by the Ministry of Science, ICT & Future Planning (MSIP) (NRF-2014R1A1A1005727) and the Engineering Research Center of Excellence Program of Korea funded by the MSIP/NRF of Korea (NRF-2014R1A5A1009799).

Notes and references

- C. H. W. Vos and L. K. Koopal, *J. Colloid Interface Sci.*, 1985, **105**, 183-196.
- W. H. Van Riemsdijk, G. H. Bolt, L. K. Koopal and J. Blaakmeer, *Journal of Colloid and Interface Science*, 1986, **109**, 219-228.
- L. Song, P. R. Johnson and M. Elimelech, *Envir. Sci. Tech.*, 1994, **28**, 1164-1171.
- I. Schenker, F. T. Filser, L. J. Gauckler, T. Aste and H. J. Herrmann, *Phys. Rev. E.*, 2009, **80**, 021302.
- J. Y. Chen, C.-H. Ko, S. Bhattacharjee and M. Elimelech, *Colloid. Surfaces. A.*, 2001, **191**, 3-15.
- M. Bendersky and J. M. Davis, *J. Colloid Interf. Sci.*, 2011, **353**, 87-97.
- M. Piech and J. Y. Walz, *J. Colloid Interf. Sci.*, 2000, **225**, 134-146.
- Y. Ji, Y. Zhang, M. Gao, Z. Yuan, Y. Xia, C. Jin, B. Tao, C. Chen, Q. Jia and Y. Lin, *Scientific Reports*, 2014, **4**, 4854.
- D. M. Kaz, R. McGorty, M. Mani, M. P. Brenner and V. N. Manoharan, *Nat. Mater.*, 2012, **11**, 138-142.
- J. D. Feick, N. Chukwumah, A. E. Noel and D. Velegol, *Langmuir*, 2004, **20**, 3090-3095.
- B. J. Park, J. Vermant and E. M. Furst, *Soft Matter*, 2010, **6**, 5327-5333.
- B. J. Park and D. Lee, *MRS Bulletin*, 2014, **39**, 1089-1098.
- M. Lee, D. Lee and B. J. Park, *Soft Matter*, 2015, **11**, 318-323.
- B. J. Park, J. P. Pantina, E. M. Furst, M. Oettel, S. Reynaert and J. Vermant, *Langmuir*, 2008, **24**, 1686-1694.
- A. Ashkin, *Biophys. J.*, 1992, **61**, 569-582.
- R. Aveyard, B. P. Binks, J. H. Clint, P. D. I. Fletcher, T. S. Horozov, B. Neumann, V. N. Paunov, J. Annesley, S. W. Botchway, D. Nees, A. W. Parker, A. D. Ward and A. N. Burgess, *Phys. Rev. Lett.*, 2002, **88**, 246102.
- R. Aveyard, J. H. Clint, D. Nees and V. N. Paunov, *Langmuir*, 2000, **16**, 1969-1979.
- B. P. Binks, *Curr. Opin. Colloid Interface Sci.*, 2002, **7**, 21-41.
- A. J. Hurd, *J. Phys. A.*, 1985, **45**, L1055-L1060.
- P. Pieranski, *Phys. Rev. Lett.*, 1980, **45**, 569-572.
- B. P. Binks and T. S. Horozov, *Colloidal Particles at Liquid Interfaces*, Cambridge University Press, New York, 2006.
- S. U. Pickering, *J. Chem. Soc. Trans*, 1907, **91**, 2001-2021.
- W. Ramsden, *Proc. R. Soc. London*, 1903, **72**, 156.
- S. Crossley, J. Faria, M. Shen and D. E. Resasco, *Science*, 2010, **327**, 68-72.
- E. Dickinson, *Curr. Opin. Colloid Interface Sci.*, 2010, **15**, 40-49.
- J. Frelichowska, M.-A. Bolzinger, J.-P. Valour, H. Mouaziz, J. Pelletier and Y. Chevalier, *Int. J. Pharm.*, 2009, 368, 7-15.
- A. P. Sullivan and P. K. Kilpatrick, *Ind. Eng. Chem. Res.*, 2002, **41**, 3389-3404.
- A. R. Studart, U. T. Gonzenbach, I. Akartuna, E. Tervoort and L. J. Gauckler, *J. Mater. Chem.*, 2007, **17**, 3283-3289.
- K. J. Stebe, E. Lewandowski and M. Ghosh, *Science*, 2009, **325**, 159-160.
- M. Cavallaro, L. Botto, E. P. Lewandowski, M. Wang and K. J. Stebe, *Proc. Natl. Acad. Sci.*, 2011, **108**, 20923-20928.
- A. R. Bausch, M. J. Bowick, A. Cacciuto, A. D. Dinsmore, M. F. Hsu, D. R. Nelson, M. G. Nikolaides, A. Travasset and D. A. Weitz, *Science*, 2003, **299**, 1716-1718.
- A. Pertsinidis and X. S. Ling, *Nature*, 2001, **413**, 147-150.
- W. T. M. Irvine, V. Vitelli and P. M. Chaikin, *Nature*, 2010, **468**, 947-951.

34. B. J. Park and D. Lee, *Langmuir*, 2013, **29**, 9662-9667.
35. K. Masschaele, B. J. Park, E. M. Furst, J. Fransaer and J. Vermant, *Phys. Rev. Lett.*, 2010, **105**, 048303.
36. M. Oettel and S. Dietrich, *Langmuir*, 2008, **24**, 1425-1441.
37. V. N. Paunov, *Langmuir*, 2003, **19**, 7970-7976.
38. J. C. Burton, F. M. Huisman, P. Alison, D. Rogerson and P. Taborek, *Langmuir*, 2010, **26**, 15316-15324.
39. B. J. Park, B. Lee and T. Yu, *Soft Matter*, 2014, **10**, 9675-9680.

Table of contents entry

The role of heterogeneity of the self-potentials in the assembly of particles at the fluid-fluid interface is characterized.

